scientific reports

Check for updates

OPEN

Efficiency enhancement of solar PV panel by incorporating wickless loop heat pipes with plate type evaporator

N. Nethaji[1], R. Suresh Kumar[2], N. Jayanthi[3], G. Murali[4], P. V. Elumalai[5], M. Murugan[6], S. Prabhakar[7]✉ & Jin Zhang[8]

The increasing global demand for energy necessitates the exploration of novel and sustainable energy sources. Solar power generation has emerged as one of the fastest-growing energy sectors worldwide. However, the performance of photovoltaic (PV) cells is significantly impacted by the rise in junction temperature, which reduces conversion efficiency. This study investigates the integration of Wick Loop Heat Pipes with Plate-type Evaporators (WLHP-PE) to mitigate the heat accumulation in solar panels, thereby enhancing their efficiency. A rolled bond evaporator plate, mounted at the rear surface of the solar panel, serves as the evaporator for the WLHP-PE system. Acetone, employed as the working fluid, is filled to an optimal level within the WLHP-PE to absorb heat from the panel's junction. Upon heating, the liquid acetone vaporizes, transporting thermal energy to a condenser section immersed in a water bath. The condenser dissipates heat to the water, causing the acetone vapour to condense back into liquid form, completing the cycle. Experimental results demonstrate that the WLHP-PE system effectively reduces the panel temperature by 5 to 9 °C under given operating conditions, leading to a 10–12% improvement in the PV module's conversion efficiency. This enhancement is achieved without requiring any external power input.

Keywords WLHP, Plate type evaporator, Conversion efficiency, Heat dissipation, Acetone medium, Junction temperature, Energy efficiency

List of symbols

C_h	Convective heat transfer coefficient (W/m^2)
q_C	Convective heat transfer (W/m^2)
Q_I	Electricity power (W/m^2)
Q_{LHP}	Heat transfer through LHP (W/m^2)
q_r	Normal radiation (W/m^2)
q_R	Radiative heat transfer (W/m^2)
Q_{RSR}	Received solar radiation (W/m^2)
T	Temperature (K)
U_{wind}	Wind velocity m/s

Greek symbols

ρ	Density (kg/m^3)
η	Efficiency of the PV module
α_0	Q_{RSR}
σ_{sb}	Stefan-Boltzmann constant (W/m^2 K^4)

Roman symbols

[1]Department of Mechanical Engineering, Government Polytechnic College, Palacode, Tamilnadu, India. [2]Department of Mechanical Engineering, R.M.K. Engineering College, Kavaraipettai, Tamilnadu, India. [3]Department of Physics, R.M.K. College of Engineering and Technology, Puduvoyal, Tamilnadu, India. [4]Department of Mechanical Engineering, Koneru Lakshmaiah Education Foundation, Green Fields, Vaddeswaram, Guntur, Andhra Pradesh 522502, India. [5]Department of Mechanical Engineering, Aditya University, Surampalem, India. [6]Department of Mechanical Engineering, Vivekanandha College of Engineering for Women, Tiruchengode, Namakkal, Tamilnadu 637205, India. [7]Department of Mechanical Engineering, Wollo University, Dessie, Ethiopia. [8]Faculty of Education, Shinawatra University, Bang Toei, Thailand. ✉email: prabhakar@kiot.edu.et

a	Ambient
N_u	Nusselt number
P_r	Prandtl number
R_a	Rayleigh number

Fossil fuels consumption which not only threatens the environment by emitting carbon and also getting depleted in an alarming way. Hence the day to day growing need for the electricity drives us towards the alternative renewable sources like solar energy[1,2]. Over 80% of the world's electricity is still generated from fossil fuels, which produce harmful emissions. Solar PV is a very promising and attracting source for generating power for industrial or residential applications[3]. In tropical countries like India, the effective utilization of solar energy has become imperative, presenting a significant technical challenge. When sunlight falls on PV cells composed of p-n junction semiconductors—it generates photons to direct current (DC) electricity through the photovoltaic effect[4]. Efficiency of commercially available PV module cells typically ranges between 15% and 18%. The remaining 72% of solar radiation is partially reflected into the atmosphere and converted into heat which itself increases the temperature of the PV module[5]. Semiconductor cells have series and parallel resistance. When temperature increases, the series resistance increases, which reduces the output power[6]. In other words, high temperature balances the charges in the semiconductor material, by reducing the magnitude of the electric field which itself inhibit the charge separation, resulting in the reduction of the voltage across the cell[7]. The power generation of the PV module decreases 0.4–0.5% for every one degree increase in the temperature of the solar cells[8]. Moreover, prolonged exposure to elevated heat condition degrades the PV cells. Therefore PV module cooling is quite important[9]. It also helps to increase the life of the solar cells by reducing thermal stress on the solar cells[10].

Overview of cooling techniques (conventional → advanced)

Different techniques are applied actively and passively to transfer the heat in PV modules represented in Fig. 1. In active techniques, external energy is supplied to circulate the coolant air or water to remove the excessive heat generated in the PV module. On the contrary, the passive techniques which do not use any mechanical pumps or blowers to remove the heat from the PV module which rather depends on natural radiation, conduction and convection modes[11]. The passive cooling mode is much preferred rather than active cooling since the former removes heat and rejects the same to atmosphere with no or minimal loss[12].

Even though the air cooling and water cooling techniques are commonly used, the Phase Change Material (PCM) based passive cooling method is gaining interest over the years, for its effectiveness[11]. Phase change materials (PCM) reduces the operating temperature of PV panel surface, to attain the higher electrical efficiency. As the heat stored in the PCM reaches the phase change temperature, the PCM starts to melt, the temperature becomes established until the process of melting is completed[13]. Experimental findings by Murali et al.[14] report up to a 60.37% increase in productivity and a 68.29% rise in efficiency, validating the effectiveness of Nano PCM in solar PV thermal enhancement. Furthermore, the integration of PCMs together with other cooling techniques like pulsating heat pipes effectively cools down the PV panel, thus ensuring its lower temperature and higher photoelectric transformation efficiency[15]. Many hindrances including the fixed thickness of the encapsulation and the amount of PCM included, integrating PCMs in the PV systems can be a solution in improving the efficiency and durability of solar energy in fulfilling the sustainable energy solutions[16]. Altogether, integrating PCMs in PV systems is an effective way to minimize efficiency reduction due to high temperatures, thus regulating the development of solar energy technologies[17,18]. WLHP with plate type evaporators contribute to increased efficiency of solar PV panels through proper thermal control. Steady-state experiments also show that thermosyphon heat pipes can cool the PV modules by about 6 °C based on comparative measurements

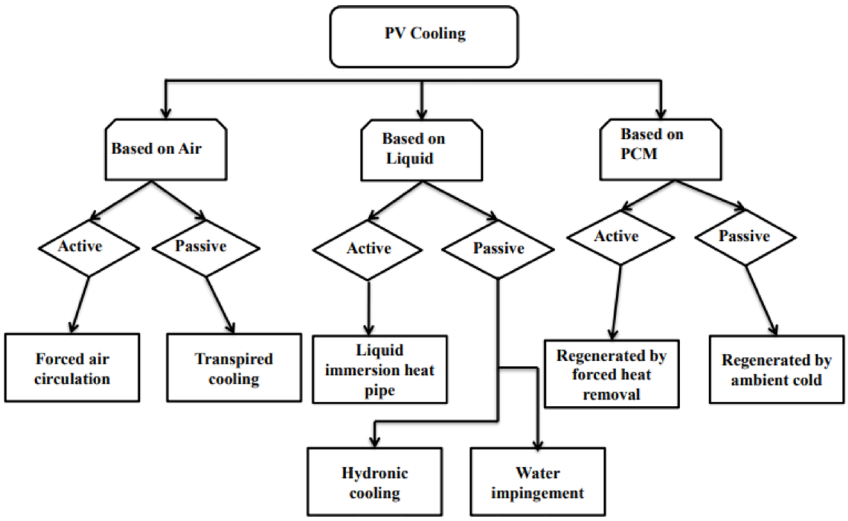


Fig. 1. PV cooling techniques[12].

of long-term efficiencies with uncooled and cooled PV panels[19]. One dimensional Enhanced Conduction Model was proposed by Mahmoud B.Elsheniti et al.[20]. A hybrid PV thermal system with nanofluid cooling was experimentally investigated using Triangular fuzzy numbers (TFN) and TOPSIS to evaluate its operating performance like conversion efficiency, surface temperature and entropy generation by Ibrahim Ahmed Qeays et al.[21]. They carried out simulation studied on PV/PCM models and reported good correlation with the already published data. A numerical and experimental validation by Zainal Arifin et al.[22] suggest that usage of Aluminium heat sink led to enhancement of open- circuit voltage and maximum power point by 10% and 18.6% respectively. A triangular proposal is proposed by Tao Ma et al.[23] on PV-PCM system properties, selection and strategy of application. Perforated Aluminium Plate was incorporated in the PV panel to enhance the production of electric current by 120% and surface temperature reduction by more than 10 °C Bizzy et al.[24]. A mathematical algorithm was developed for designing the flow dimensions of a cooling system for PV panel by Roozbeh Yousefnejad et al.[25]. The CFD simulation analysis showed 1.7 K as difference in cooling water outlet temperature.

Kianifard .S et al.[26] designed a cooling system for PV/T collector system and carryout experimental trials and compared the results with the simulated results. They reported good agreement with 15% error. A dynamic model for irrigation cooling system for PV panel was designed for three PV panels and their performance were experimentally evaluated for intermittent irrigation by German Osama-Pinto et al.[27]. They reported reasonable agreement on performance with regard to surface temperature and power production. Mohammad Alhuvi Nazari et al.[28] carried out experimental investigation on pulsating heat pipes by using Graphine Oxide nano-fluid as working medium in evaluating its thermal performance.For four different concentrations their experiment as shown a decrease of 42% thermal resistance and considerable enhancement in thermal conductivity.

A review work on applications of pulsating heat pipes was carried out by Mohammad Alhuvi Nazari et al.[29]. In their work they reported that the application of cryogenic pulsating heat pipe can achieve 12,000 W/mK of thermal conductivity.

By using neural networks, the thermal performance of pulsating heat pipes were carried out by Mohammad Hossein Ahmadi et al.[30]. They used ethanol as the working fluid and reported radial bias function model as highest precision among the all models used for evaluation of thermal resistance prediction.

Passive cooling using thermosiphon effect

Thermosiphon effect is a gravity assisted heat transport system which transfers the heat from one location to another. This system facilitates the working fluid circulation without the need of mechanical pump, which consists of two heat exchangers named a condenser and an evaporator connected together. The heat exchanger system is primarily evacuated and filled with working fluid. Evaporator section consists of working fluid in its liquid phase and the condenser contains saturated vapour. The heat in PV module evaporates the working fluid in the heat pipe, simultaneously increasing the pressure in whole system. As the condenser section is externally cooled by the water immersion technique, saturated vapour condenses into liquid, which itself returns to the evaporator sections due to gravity and tilt effect. As a result considerable amount of heat is transferred from the evaporator to the condenser[31].

Motivation and novelty of WLHP-PE

While various cooling strategies such as thermosiphon systems, nanofluids, and hybrid PV/T collectors have shown promise in reducing PV module temperature, many involve complex configurations, moving parts, or active power input. The specific gap this study addresses is the need for a passive, low-resistance, and uniformly effective cooling system that is both scalable and energy-efficient without compromising on performance. In this work, we propose a WLHP-PE system, directly integrated onto the rear surface of the PV panel using thermally conductive adhesive. Unlike conventional heat pipe systems that rely on wick structures, our wickless design drastically reduces flow resistance, enhancing heat transfer performance. The plate-and-tube evaporator, made from aluminum for optimal conductivity, ensures uniform cooling across the panel surface. We also use acetone as the working fluid due to its favorable thermo-physical properties, enabling efficient phase change and heat transport. The WLHP-PE operates entirely passively under gravity and thermosiphon effects, eliminating the need for external pumps or power. This makes it especially suitable for remote or off-grid applications. The novelty of our work lies not only in the passive wickless design but also in its practical implementation: three plate-type WLHPs connected to a common header ensure consistent temperature control and system simplicity. Compared to more complex systems like nanofluid or hybrid cooling, WLHP-PE offers a simpler, cost-effective, and easily manufactural alternative with comparable efficiency improvements, filling a critical gap in passive PV thermal management.

This study presents a novel approach to PV module cooling through the design and integration of a WLHP-PE. The system employs rolled-bond aluminium evaporator plates without wick structures, which reduces internal flow resistance and enables efficient passive operation using the gravity-assisted thermosiphon effect. A unique configuration of three parallel evaporator units connected to a common condenser promotes uniform temperature distribution and enhanced cooling performance across the PV surface. The use of acetone as the working fluid, combined with the system's compatibility with conventional PV modules, provides a scalable, cost-effective, and power-free thermal management solution.

Energy balance equation for PV panel

The temperature of the PV module surface is obtained by energy balance equation. The part of the absorbed solar energy is radiated into the atmosphere and transferred by convection heat transfer. The remaining part of energy is converted into electricity and used to increase the internal energy of the PV module. The heat balance for the PV module, before and after incorporation of WLHP-PE is presented in Fig. 2a and b.

PV module energy balance equation is,

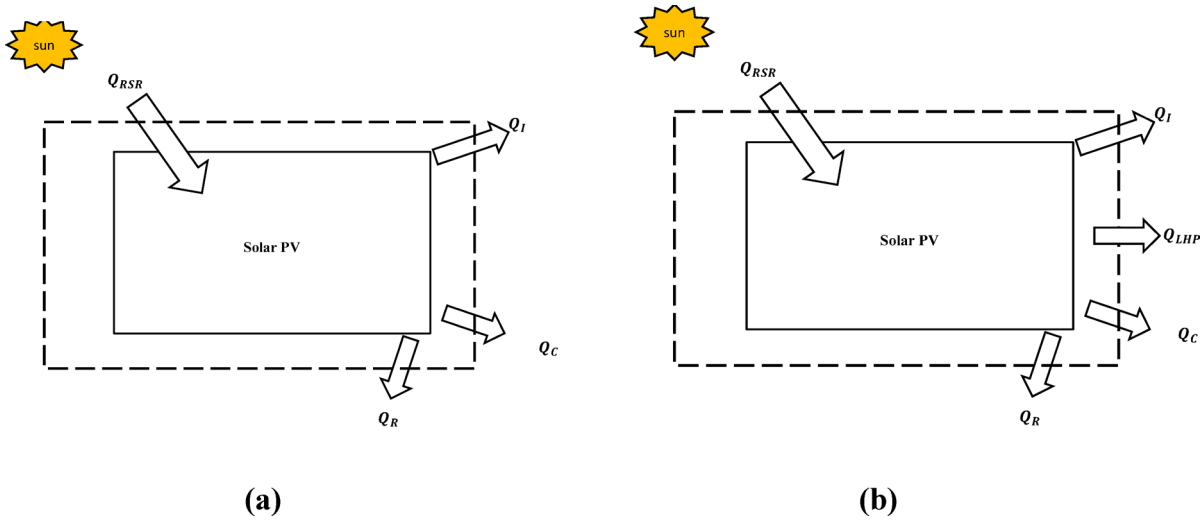


Fig. 2. (**a**) The heat balance for the PV module, before incorporation of WLHP-PE, (**b**) the heat balance for the PV module, after incorporation of WLHP-PE.

$$Q_{RSR} = Q_I + q_C + q_R + Q_{LHP} \tag{1}$$

The received solar radiation (Q_{RSR}) is calculated by

$$\mathrm{Q_{RSR}} = \alpha_0 q_\mathrm{r} \tag{2}$$

Where, α_0 is the absorption rate of PV cell and q_r is the normal solar radiation on the PV panel.

The generated power is obtained by

$$\mathrm{Q_I} = \eta q_\mathrm{r} \tag{3}$$

Where, η represents the efficiency of the PV panel. The Eq. (3) shows that the efficiency of the PV panel is influenced by its working temperature. The surface temperature of the PV module and its efficiency is correlated as[32],

$$\eta = -0.1757\mathrm{T_S} + 21.737 \tag{4}$$

Convective and Radiative heat transfer energy is given by the equations as, q_c & q_r is the convective and radiative heat flux.

$$\mathrm{q_C} = \mathrm{C_h}\left(\mathrm{T_S} - \mathrm{T_A}\right) \tag{5}$$

$$\mathrm{q_R} = 2\varepsilon_0\sigma_{\mathrm{sb}}\left(\mathrm{T_S}^4 - \mathrm{T_A}^4\right) \tag{6}$$

Where, ϵ_0 is the emissivity of the PV module surface and σ_{sb} is Stefan-Boltzmann constant. C_h is the convective heat transfer co-efficient on the backside of the PV module and the same is calculated as follows[10].

$$\mathrm{Nu}* = \left\{0.825 + \frac{0.387Ra^{1.6}}{\left[1 + (0.492/Pr)^{9/16}\right]^{8/27}}\right\}^2 \tag{7}$$

The upper side convective heat transfer is estimated by.

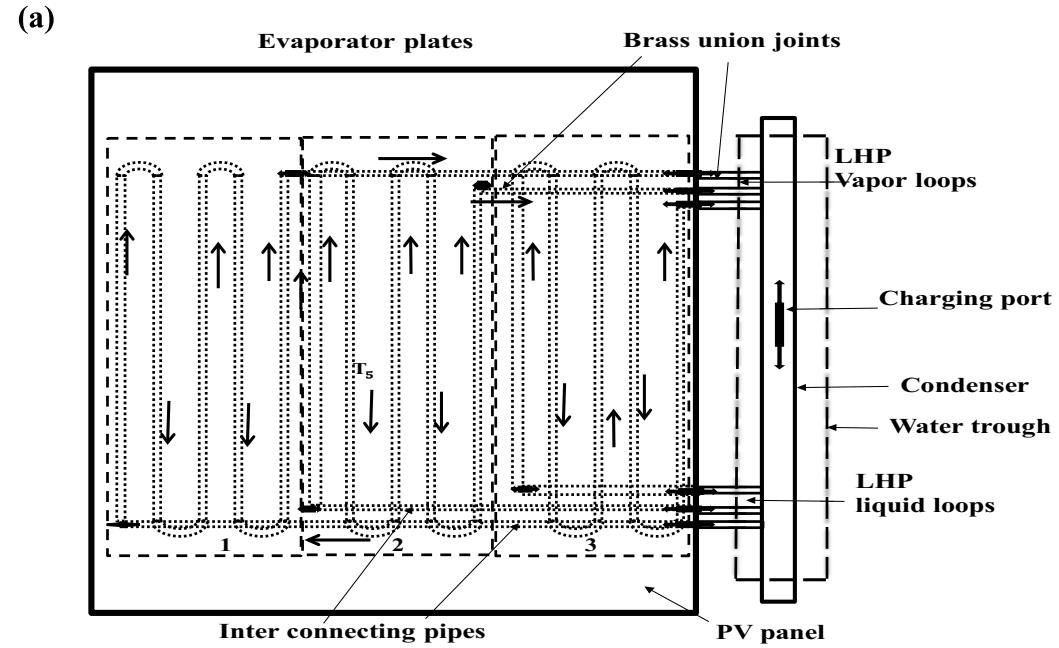
$$\mathrm{h} = 2.8 + 3.8\ \mathrm{U_{wind}}$$

$$Q_{RSR} = Q_I + q_C + q_R + Q_{LHP}$$

Experimental methodology

The material for the heat pipe is selected based on the compatibility of working fluid. Copper and Aluminium are the best suitable materials for the heat pipe which operates efficiently in the temperature of -20 to 100 °C[33]. The Construction of WLHPs with plate type Evaporator as shown in Fig. 3a, The PV panel is fitted with three Aluminium rolled bond evaporator plates to form WLHP-PE as shown in Fig. 3b. The construction details as shown in shown in Table 1.

In our study, acetone was used as the working fluid in the WLHP-PE system due to its favourable thermophysical properties, such as low boiling point and high latent heat, which make it effective for passive



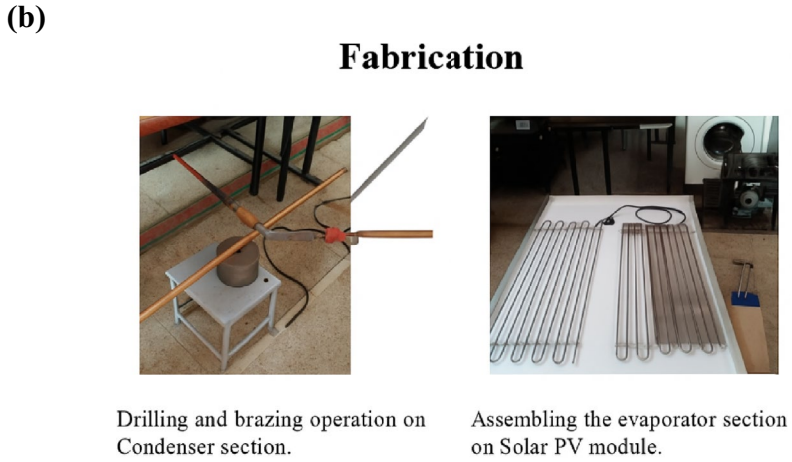


Fig. 3. (**a**) Schematic diagram of the construction of wickless loop heat pipes with plate type evaporator. (**b**) Photographic view of construction of wickless loop heat pipes with plate type evaporator.

Component	Material	Dimension	Fabrication
Evaporator plates-3 number	Rolled bond aluminium with 3 passes each	(1800 × 330)mm Pass ID 6.35 mm	3 plates attached to the bottom surface of panel with thermal adhesive
Liquid loops-3 number	Copper	ID 5.5 mm, OD 6.5 mm, length 386 mm,416 mm and 436 mm each	Flare nuts and union joints brass material
Vapour loops 3-number	Copper	ID 6.5 mm, OD 7.5 mm, length 376 mm,406 mm and 426 mm each	Flare nuts and union joints brass material
Condenser pipe-one number	Copper	23.5 mm ID, 25 mm OD and 1800 mm	Ends sealed by brazing operation
Condenser cooling trough-one number	PVC	60 mm diameter Semi hallow cylindrical 2000 mm long	PVC pipe solvent cement

Table 1. Construction details of the WLHP-PE.

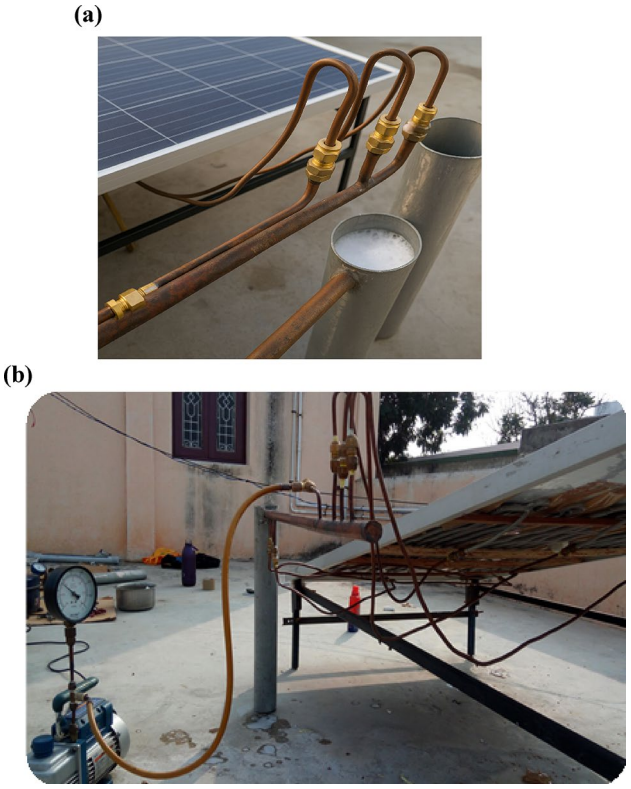


Fig. 4. (**a**) Physical view of leak testing of WLHPs. (**b**) Physical view of vacumizing of WLHPs.

Property	Value
Boiling point	56.05 °C
Melting point	− 94.8 °C
Density	0.791 g/cm^3
Solubility	Miscible with water, alcohol, and most organic solvents
Heat of vaporization	30.99 kJ/mol at 25 °C
Auto ignition temperature	465 °C
Flashpoint	− 20 °C
Flammability limits (in air)	2.5–12.8% by volume
Heat of formation (gas)	− 218.0 kJ/mol
Heat of formation (liquid)	− 249 kJ/mol
Heat of fusion	5.7 kJ/mol
Heat of evaporation	31.0 kJ/mol
Cp (constant pressure heat capacity, liquid)	125.45 J/mol K at 298.15 K
Cp (constant pressure heat capacity, gas)	75.32 J/mol K at 300 K

Table 2. Thermophyscial properties of the acetone.

heat transfer. Nitrogen, on the other hand, was used only during the leak testing phase—charged into the loop at 10 bar to check the integrity of joints and fittings using soap solution as shown in Fig. 4a. Leak test on all the union joints between condenser section and evaporator section. In this test compressed air is charged on the loop heat pipe with particular pressure using the single stage reciprocating compressor. After leak testing the vacuuming and dehydration were carried out simultaneously using a double stage vacuum pump. The vacuum level was at 300 Microns as shown in Fig. 4b. Table 2 shows the properties of Acetone.

Experimental setup

The experimental setup involves a 260 W polycrystalline PV module integrated with three WLHP-PE, each consisting of a rolled-bond aluminium plate with three internal passes. These evaporators are attached to the rear surface of the PV panel using high thermal conductivity adhesive to ensure effective thermal contact. Copper tubes with inner diameters of 6.5 mm inner diameter vapor loops and 5.5 mm inner diameter liquid

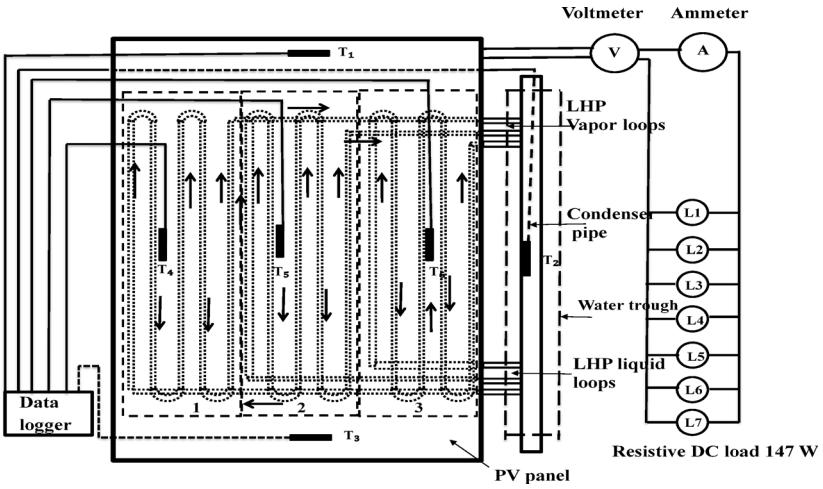


Fig. 5. Schematic diagram of the experimental setup: 1, 2, and 3 is WLHP-PEs, and T1, T2, T3, T4, T5, and T6-Resistance temperature detector sensors.

Instruments	Manufacturer	Model	Accuracy (full scale)
Ammeter(0–25 A DC)	Yokins	DD-DA100-09	±1%
Voltmeter(0–100 V DC)	Yokins	DD-DV500-09	± 1%
RTD sensors and DATA logger – sub zero	A.S.Controls, Mumbai (ISO 9001-2008)	Probe type RTD sensors SZ DL16000 RS 485	± 2%

Table 3. Accuracy and uncertainty of measurements.

loops connect the evaporators to a common copper condenser pipe 23.5 mm ID, 25 mm OD, 1800 mm length), assembled using brass flare nuts and union joints sealed with Teflon tape. The condenser is fabricated by brazing and immersed in a water bath for heat dissipation. Nitrogen gas was initially charged at 10 bar to conduct leak testing, after which the system was evacuated to 300 microns using a double-stage vacuum pump. Acetone, selected for its favorable thermophysical properties, was charged to 50% of the evaporator volume as the working fluid, enabling passive circulation through thermosiphon effect. Temperature measurements are obtained from six calibrated RTD sensors connected to a Sub Zero SZ DL16000 RS 485 data logger, while electrical output (voltage and current) is monitored using Yokins DC ammeter and voltmeter. The entire assembly is mounted on a fixed frame inclined at approximately 13° to maintain consistent solar exposure during the experimental trials.

The WLHP-PE cylindrical condenser section is fabricated by brazing operation. The working fluid and its pressure are chosen based on the saturation temperature between the condenser and evaporator temperature[34]. The whole setup is fitted under the solar panel using high conductive thermal adhesive. In the present study, the evaporator plates were attached to the backside of the PV panel using a high thermal conductivity adhesive, specifically selected to ensure intimate contact and minimize interfacial thermal resistance. Although direct measurement of the thermal contact resistance was not conducted in this work, care was taken during assembly to ensure uniform adhesion and elimination of air gaps, which are primary contributors to elevated contact resistance. We acknowledge that thermal contact resistance can significantly influence the effectiveness of heat transfer, particularly in passive systems like WLHP-PE, where the driving temperature difference is modest. A high interfacial resistance would reduce the rate at which heat is transferred from the PV module to the working fluid, potentially undercutting the efficiency gains from the cooling system.

As the boiling point of the coolant is predominantly determined by the vacuum in the pipes, a small double stage vacuum pump is used for vacuuming the WLHP-PE to the level of 20 Pa.

Instrumentation

An Ammeter with range of (0–25 A) DC, a DC voltmeter of range (0–100 V) and a six channel tempararture monitor with RTD sensors are mounted at specific locations as shown in the experimental setup Fig. 5. The RTD sensors and data logger (Sub Zero SZ DL16000 RS 485) were calibrated prior to the experiments. The calibration was performed using a standard temperature calibration bath, and the sensors were cross-verified against a certified reference thermometer with known accuracy. The accuracy of measurements and uncertainity of these instruments are tabuated in Table 3.

Calculation for working fluid charge

Volume of the evaporator section:

$$\text{Diameter of evaporator pipe d} = 6.35 \text{ mm}$$

$$\text{Radius r} = 3.175 \text{ mm}$$

$$\text{Length of each pass of evaporator tube l} = 1010 \text{ mm}$$

$$\text{Volume of the each section in evaporator} = \pi r^2 l$$
$$= 3.14 \times (3.175)^2 \times 1010$$
$$= 31985 \text{ mm}^3$$

$$\text{Volume of the total 14 evaporator section} = 14 \times 31.985$$
$$= 447.8 \text{ cm}^3$$

The working medium, acetone is charged in the WLHP-PE to the level of 50% of its total evaporator volume.

The gravity and tilt effect assist the continuous circulation of liquid through the WLHP-PE loop. The temperature gradient which exists between the condenser and evaporator section facilitates the phase changing and flow circulation process of working fluid[32]. During the liquid flow phase of the coolant, it absorbs the heat generated in the solar panel and becomes vapour. This vapour moves towards the condenser section, which is immersed in the water bath. This immersion cooling method helps the vapour to liberate substantial amount heat which is absorbed in the PV module and to regain its liquid phase.

The chassis, for setting up the solar PV module is designed and fabricated as per the tilt requirement of PV module. RTD sensors are placed under the solar PV module setup to measure the temperature. The following photographic views Fig. 6a–d, shows the physical experimental setup and the connected instrumentation.

Voltmeter and ammeter are properly connected in the DC load with the module. The evaporator section of WLHP-PE are attached under the PV-module and condenser section of immersed in water bath.

Experimental trial and data collection

The PV module with experimental WLHP-PE setup is placed in Nesevalar colony Dharmapuri, Tamilnadu (N 12° 7' 38.6652", E 78° 9' 28.9224").India, at corresponding latitude of 13°. The PV module was installed at a fixed tilt angle of 11°, aligned with the local latitude to maximize solar energy absorption. This angle was chosen based on the optimal inclination for the geographic location of the test site to maximize solar irradiance. The setup was fabricated and assembled as Fig. 3a. The trail was carried out without WLHP from July 18, 19, 20-2022 after connecting DC load of 147 W and the experiments were conducted for 2 h per day over 3 days, between 10:30 AM and 12:30 PM, during peak solar radiation. While this duration allowed observation of thermal effects, we acknowledge that a longer and more continuous testing period would provide a more comprehensive assessment of the cooling system's effectiveness. Open circuit voltage (V_{OC}), average temperature of panel (T), Voltage with load (V_L), Current with load (I_L) were recorded with the instruments attached to the setup and the data logger. The average data is taken for calculation purpose and graph are drawn for inference. The above procedure is repeated on the setup after incorporating WLHP at bottom of the panel using thermal adhesive as depicted in Figs. 4a and b and 5 during July 21, 22 and 23 of 2022. The specifications of the PV panel as shown in Table 4. The data collected were used for evaluating the performance of the PV panel with WLHP-PE. Electrical nominal at 25 °C and Standard test conditions.

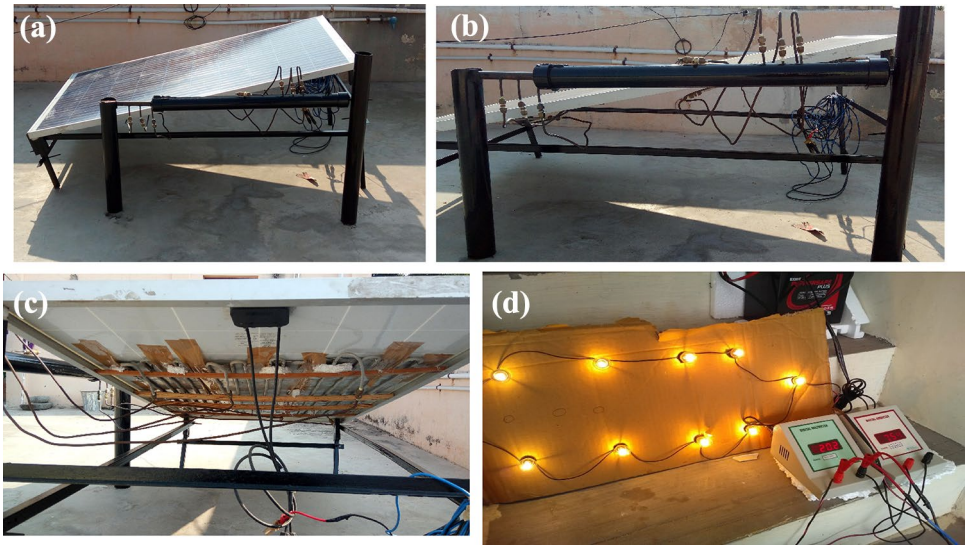


Fig. 6. (**a**) A photographic side view of the experimental setup. (**b**) A photographic view of the Condenser, supply and return loops of WLHP-PE. (**c**) A photographic bottom view of the panel with WLHP-PE. (**d**) A photographic view of the Loading, Voltage and current Measurement instrumentation.

Description	Specifications
Product description LVS-260	
Maximum power at standard test condition (Pmax)	260 W
Tolerance	±3%
Maximum voltage (Vmp)	30.88 V
Open circuit voltage (V_{OC})	37 V
Current at maximum power (Imp)	8.54 A
Short circuit current (Isc)	9.07 A
Solar irradiance	1000 (W/m^2)
Module temperature	25 °C
Spectrum AM	1.5
Voltage VOC	(– 379% of Voc/K)
Current ISC	(– 0.0396% of Isc/K)
Power P max	(– 0.48% /K)
Maximum system voltage	1000 DC
Type of solar cell	Polycrystalline silicon

Table 4. Specifications of the PV panel.

Component	Material	Dimension	Cost
Evaporator plates-3 number	Rolled bond aluminium with 3 passes each	(1800 × 330)mm Pass ID 6.35 mm	3 Numbers at the rate of Rs.1250 = Rs.3750
Liquid loops-3 number	Copper	ID 5.5 mm, OD 6.5 mm, length 386 mm,416 mm and 436 mm each	3 Numbers at the rate of Rs.650 = Rs.1950
Vapour loops 3-number	Copper	ID 6.5 mm, OD 7.5 mm, length 376 mm,406 mm and 426 mm each	3 Numbers at the rate of Rs.650 = Rs.1950
Condenser pipe-one number	Copper	23.5 mm ID, 25 mm OD and 1800 mm	1 Number at the rate of Rs.2000
Condenser cooling trough-one number	PVC	60 mm diameter ,1.5 mm thick Semi hallow cylindrical	Fabrication cost Rs.950
3 numbers fabrication, brazing, leak testing, vacuumizing of WLHP-PE and charging of working fluid (acetone)	Labour work, leak check, Brazing	As stated above	Assembly and testing of WLHP-PE 3 numbers at the rate of Rs.1200 = Rs.3600
			Miscellaneous charges Rs.3000
Total cost of incorporation of WLHP-PE in the PV panel including miscellaneous charges = Rs.17,200			

Table 5. Cost breakdown for WLHP-PE integration.

Cost analysis, payback period and life cycle assessment

The total cost of incorporating the WLHP-PE system into the PV panel, including all components and fabrication charges, is approximately Rs 17,200 as shown in Table 5. A significant improvement in the energy output of the PV panel was observed after the integration of the cooling system.

Energy Output Comparison:

- Before Integration of Cooling System:
  - Power output = 122.13 Watts.
  - Operating hours = 6 h/day × 30 days = 180 h/month.
  - Monthly energy production = 122.13 × 180 = 21.983 kWh/month.
- After Integration of Cooling System:
  - Power output = 166.98 Watts.
  - Monthly energy production = 166.98 × 180 = 30.56 kWh/month.
- Additional Energy Generated:
  - = 30.56–21.983 = 8.576 kWh/month (approx.)

Cost Savings:

- Commercial electricity rate (India): Rs.12 / unit (1 unit = 1 kWh).
- Monthly Savings = 8.576 × 12 = Rs.102.91.
- Annual Savings = Rs.102.91 × 12 = Rs.1,234.92.
- Total Savings over 25-year panel lifespan = Rs.1,234.92 × 25 = Rs.30,873.

η	Maximum error S_η %
9.90	± 1.98
10.20	± 1.08
10.30	± 0.80
10.60	± 0.56
10.90	± 0.46
11.10	± 0.22
11.40	± 0.18
11.70	± 0.16
12.00	± 0.15

Table 6. Experimental error range.

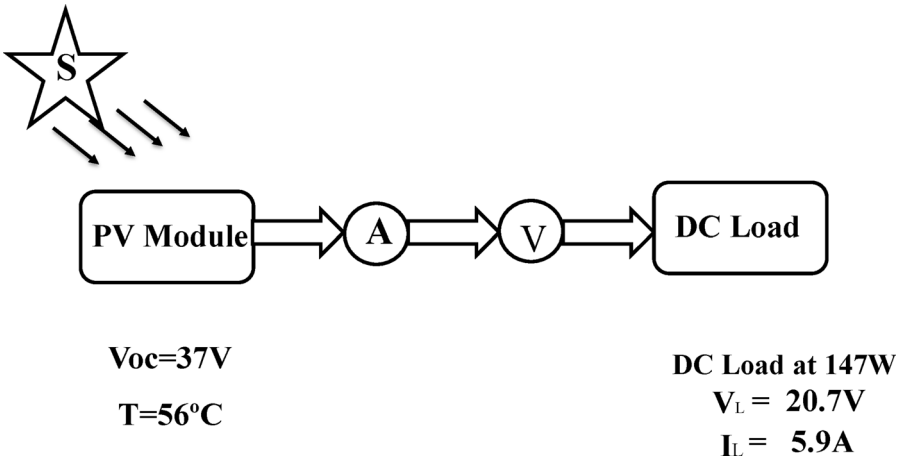


Fig. 7. Configuration of without WLHP-PE.

Payback Period:

The life cycle cost analysis and payback period were evaluated using basic economic calculations based on the initial system cost, monthly energy savings, and electricity tariff. The payback period was calculated using the formula[35].

$$\text{Payback Period} = \text{Total System Cost}/\text{Annual Savings} \tag{8}$$

- Estimated cost of WLHP cooling system integration = Rs.17,200 (example – please insert actual value if different).
- Payback Time = 17,200 / 1,234.92 ≈ 13.93 years (~ 13 years and 11 months).

Error analysis

The main uncertainty source for the calculated parameter conversion efficiency originates from temperature data from Pt 100 RTD sensors, the ammeter and a data logger (Sub Zero SZ DL 16000 RS 485).The involvement of uncertainties with these readings are detailed in Table 6.

As per Taylor's uncertainty theory[34], the uncertainties of propagation *S*) can be computed from

$$S_\eta = \eta * \sqrt{\left(\frac{S_{Eb-Ea}}{Eb-Ea}\right)^2} \tag{9}$$

Where,

$(S_{Eb-Ea}) = \sqrt{S_{Eb}^2 + S_{Ea}^2}$: The error associated with (*Eb-Ea*), *Eb*: power generated by normal PV panel, *Ea* : power generated by WLHP-PE incorporated PV panel. By computing *S* from Eq. (9), for the experimentation range considered, the Table 5 gives maximum permissible error range.

Configurations of setup

Without WLHP-PE

Figure 7, shows the configuration of typical performance of PV panel before incorporation of the WLHP-PE setup. For the given operating conditions the performance nominal for the normal PV panel is shown below.

With WLHP-PE

Figure 8, shows the configuration of typical performance of PV panel after incorporation of the WLHP-PE setup. For the given operating conditions the performance nominal for the WLHP-PE PV panel is shown below.

Results and discussions

The observations are performed on the commercially available 250 W solar panel. Parameters like temperature, current and voltage readings are noted down for the DC load. Pt100 Resistance Temperature Detectors (RTD) sensors are used to measure the temperature. The data collections are recorded during two different intervals of morning (10:30–11:30) and noon (14:00–15:00) two hours per day not conduct one hour conducted between 10:30 AM and 12:30 PM. While irradiance sensors were not employed, we minimized variability by conducting all experiments—both with and without WLHP-PE—during the same daily time slots (10:30–11:30 AM and 2:00–3:00 PM) over consecutive days with recorded ambient conditions (irradiance ~ 1000 W/m², wind speed 8 m/s, RH 65%) that remained largely stable.

Effects of WLHP-PE on voltage generated

Graphs are drawn with the collected data based on the trials. As evident in the Fig. 9a, from July 18, 19 and 20 of 2022 the normal PV module generates an average voltage of 23.75 V, during the trial period of 10.30–11.30 AM, Ambient temperature is 30 °C, Wind Velocity: 8 m/s, RH : 65%. After the incorporation of WLHP system in the panel the same variable is found to be an average of 25.3 V on July 21, 22 and 23 0f 2022, the trial period of 10:30 to 11:30 AM, Ambient temperature is 30 °C, Wind Velocity: 8 m/s, RH : 65%. It is concluded that this increase in voltage is due to effect of enhanced conversion efficiency of the PV panel consequent upon the reduced junction heat. Also it is proved that the WLHP-PE system that was incorporated to the PV panel is performing properly.

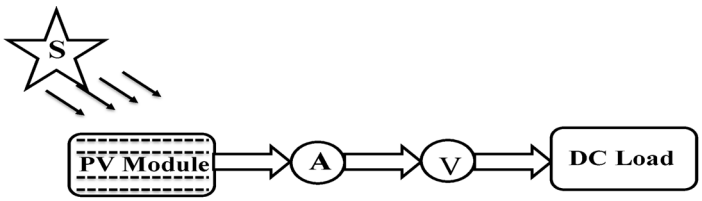
The above procedure is repeated during 2.00 pm to 3.00 pm of the above dates and the graph is drawn as below in Fig. 9b, and the average voltage found to be 17 V and 22 V respectively. With WLHP-PE Trial date: July 18, 19 &20 of 2022 trial time: 2.00 to 3.00 PM, Ambient temperature is 30 °C, wind velocity: 8 m/s, RH is 65%. Without WLHP-PE Trial date: July 21, 22 &23 of 2022 Trial time: 2.00 to 3.00 PM, ambient temperature is 30 °C wind velocity of 8 m/s, RH is 65%.

Effects of WLHP-PE on production of current

Graphs are plotted with the collected data based on the trials. The DC current produced during the trial period was recorded with an ammeter during the time 10.30–11.30 AM of the trial period for both WLHP-PE fitted and normal PV panel. The curve for the current value stagers over time. The increase in current value to a particular level, indicates the proper functioning of WLHP-PE system and hence enhanced cooling of PV panel, as the as shown in Fig. 10a. For given operating conditions the average current produced without WLHP-PE is found to be 6.3 A. Upon incorporating the WLHP-PE in the system the same variable is enhanced and found to be 6.7 A. With WLHP-PE Trial date: July 18, 19 &20 of 2022 trial time: 10:30 to 11:30 AM, ambient temperature is 30 °C, wind velocity: 8 m/s, RH: 65%. Without WLHP-PE Trial date: July 21, 22 &23 of 2022, trial time is 10:30 to 11:30 AM, ambient temperature: 30 °C, wind velocity: 8 m/s, RH: 65%. The above procedure is repeated during 2.00 pm to 3.00 pm and the graph is drawn as below in Fig. 10b. It is evident that this increase in current is due to effect of enhanced conversion efficiency of the PV panel consequent upon the reduced junction heat. Also it is demonstrated that the WLHP-PE system that was incorporated to the PV panel is performing properly. With WLHP-PE Trial date: July 18, 19 &20 of 2022, trial time: 2.00 to 3.00 PM, Ambient temperature is 30 °C wind velocity: 8 m/s, RH: 65%. Without WLHP-PE Trial date: July 21, 22 &23 of 2022, trial time: 2.00 to 3.00 PM, ambient temperature: 30 °C, wind Velocity: 8 m/s, RH: 65%.

Effects of WLHP-PE on PV panel temperature

Graphs are drawn with the collected data based on the trials. The Pt100 RTD sensors attached to the panel at 6 different locations record the real time temperature of the panel before and after incorporation of WLHP-PE in



Voc=37V

T=45°C

DC Load at 147W

V_L=25.3V

I_L=6.6A

Fig. 8. Configurations of with WLHP-PE.

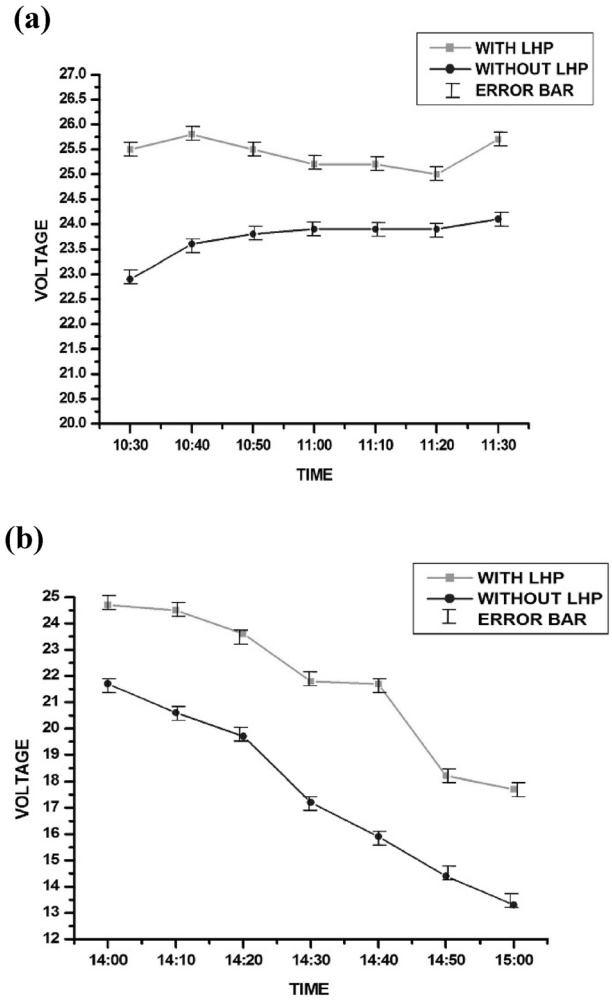


Fig. 9. (**a**) Effects of WLHP-PE on voltage generated at trail period 10:30 to 11:30 AM. (**b**) Effects of WLHP-PE on voltage generated at trail period 2:00 to 3:00 PM.

PV panel during two different time slot 10.30–11.30 AM and 2.00–3.00 PM. For the given operating conditions the average temperature is reduction is found be over 7–10 °C. The readings are tabulated and drawn as graphs as shown in Fig. 11a With WLHP-PE trial date: July 18, 19 &20 of 2022, trial time: 10:30 to 11:30 AM, ambient temperature is 30 °C, wind velocity is 8 m/s, and RH : 65%. Without WLHP-PE trial date: July 21, 22 &23 of 2022 trial time: 10:30 to 11:30 AM, ambient temperature is 30 °C, wind Velocity: 8 m/s, and RH: 65. Figure 11b, With WLHP-PE trial date: July 18, 19 &20 of 2022 trial time: 2.00 to 3.00 PM, Ambient temperature is 30 °C, wind velocity: 8 m/s, and RH: 65%. Without WLHP-PE Trial date: July 21, 22 &23 of 2022, trial time: 2.00 to 3.00 PM, ambient temperature is 30 °C, wind velocity is 8 m/s, and RH: 65%. It is arrived that this decrease in temperature is due to the incorporation of WLHP-PE system. Also it is proved that the WLHP-PE system that was incorporated to the PV panel is performing properly.

Statistical analysis and repeatability

The repeatability and statistical significance of the experimental results, the data collected over three consecutive days for both control (without WLHP-PE) and test (with WLHP-PE) conditions were subjected to statistical analysis. For each key performance metric—voltage, current, temperature, and conversion efficiency, the mean and standard deviation (σ) were calculated based on repeated daily measurements. The Table 7 shows Mean and Standard Deviation of Key Performance Parameters.

These values are now reflected with error bars in revised Figs. 9, 10, 11 and 12 to illustrate measurement variability.

ANOVA significance test

A one-way ANOVA (Analysis of Variance) was conducted to evaluate whether the performance improvements were statistically significant. The p-values for each parameter were as follows. The Table 8 shows ANOVA test results for statistical significance.

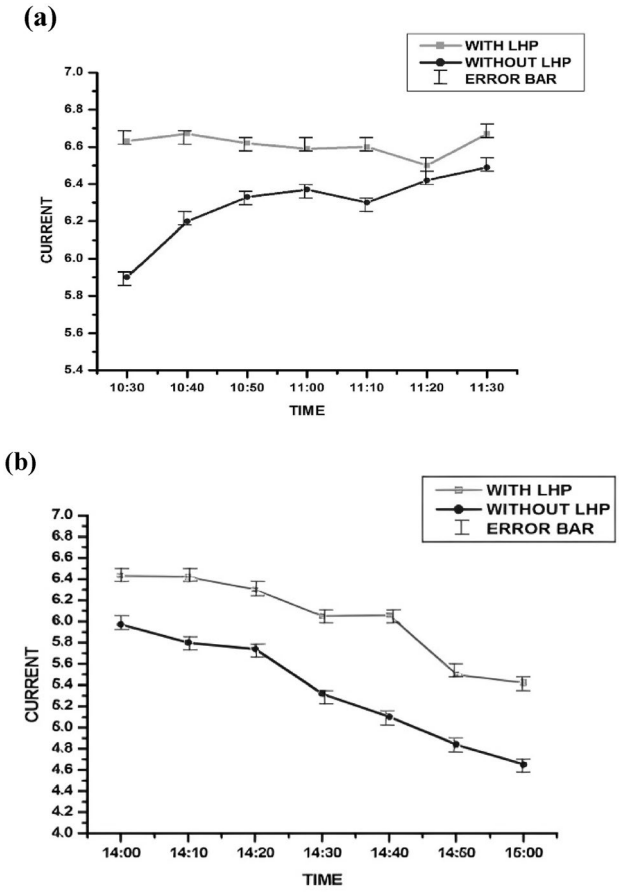


Fig. 10. (**a**) Effects of WLHP-PE on production of current at trail period 10:30 to 11:30 AM. (**b**) Effects of WLHP-PE on production of current at trail period 2:00 to 3:00 PM.

Conversion efficiency enhancement

Graphs are drawn with time against efficiency using the data collected during trials. Due to enhanced cooling of the cell junctions upon incorporation of WLHP-PE system and hence the lesser junction heating, the conversion efficeiney is found to increase as found from graph in Fig. 12. With WLHP-PE trial date: July 18,19 & 20 of 2022, trial time: 10:30 to 11:30 AM, ambient temperature is 30 °C, wind velocity: 8 m/s, RH : 65%. Without WLHP-PE trial date: July 21,22 &23 of 2022, trial time: 10:30 to 11:30AM, ambient temperature is 30 °C, wind velocity: 8 m/s, RH :65%. For the given operating conditions the average efficiency of the PV panel without LHP is found to be 10.2%. Upon extensive trials after incorporation of WLHP-PE in the setup the average efficiency of the PV panel is found to be 11.4% (Table 9). A comparison between the current findings and previous published studies.

$$\text{Efficiency } \eta = \frac{\text{Rating of the panel from the datasheet}}{\text{Area of PV module} \times \text{STC the watts per meter squared } (\text{W/m}^2)} \times 100$$

Conclusion

In this study, the effectiveness of cooling a solar PV panel by incorporating a wickless WLHP-PE was experimentally validated. The system utilizes a rolled-bond aluminium evaporator configured as a WLHP, which is partially filled with a working fluid at a filling ratio of 50%. This evaporator is securely attached to the underside of the PV panel using a thermally conductive adhesive to facilitate efficient heat transfer. The condenser section of the WLHP-PE is submerged in a water bath, ensuring effective dissipation of heat.

The experimental results demonstrate that the performance of the PV panel equipped with WLHP-PE cooling aligns closely with previously reported findings. Under the specified operating conditions:

- The output voltage of the PV panel showed a significant improvement, increasing by approximately 2 to 4 volts.
- The electric current generated by the panel increased by an additional 0.4 to 0.8 amperes.
- The junction temperature, and consequently the overall temperature of the PV panel, was reduced by 8 °C to 10 °C.
- The cooling mechanism led to an enhancement in the panel's energy conversion efficiency, with an observed improvement of 10–12%.

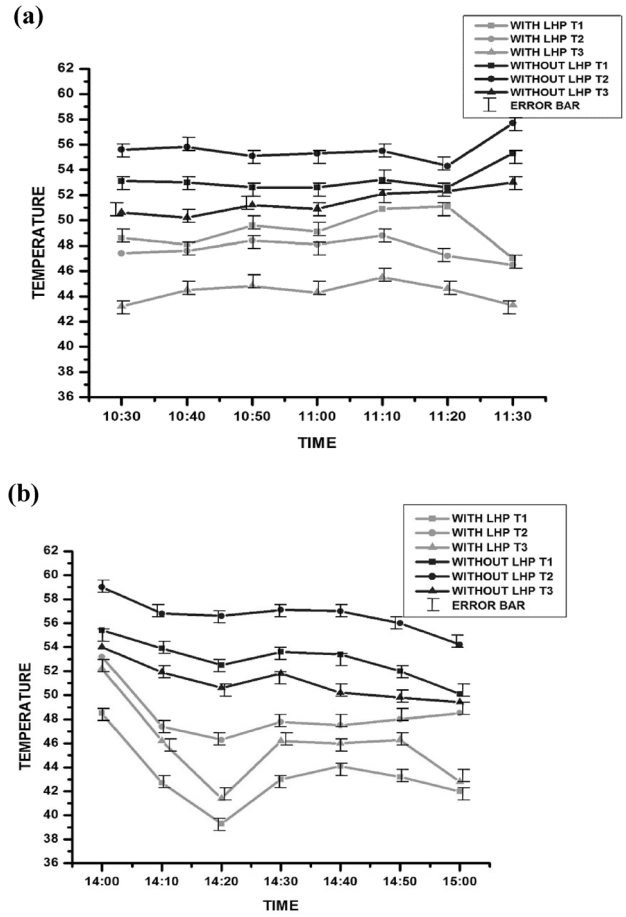


Fig. 11. (**a**) Effects of WLHP-PE on PV panel temperature at trail period 10:30 to 11:30 AM. (**b**) Effects of WLHP-PE on PV panel temperature at trail period 2:00 to 3:00 PM.

Parameter	Condition	Mean	Standard deviation (σ)
Voltage (V)	Without WLHP-PE	23.75	0.37
	With WLHP-PE	25.30	0.29
Current (A)	Without WLHP-PE	6.30	0.21
	With WLHP-PE	6.70	0.18
Panel temperature (°C)	Without WLHP-PE	54.0	1.5
	With WLHP-PE	45.5	1.2
Efficiency (%)	Without WLHP-PE	10.2	0.28
	With WLHP-PE	11.4	0.24

Table 7. Mean and standard deviation of key performance parameters.

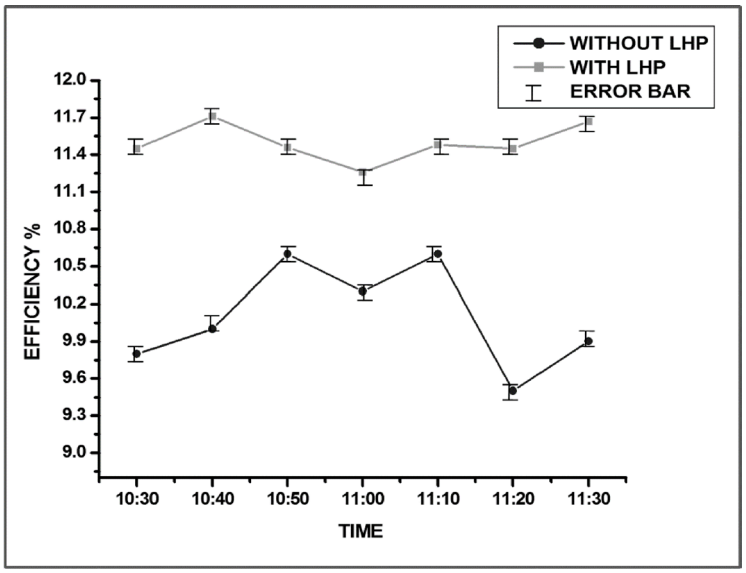


Fig. 12. Effects of WLHP-PE on PV panel efficiency.

Parameter	*P*-value
Voltage	0.007
Current	0.014
Temperature	0.003
Conversion efficiency	0.010

Table 8. ANOVA test results for statistical significance. Since all p-values are < 0.05, the differences between the control and test groups are statistically significant at the 95% confidence level, confirming that the observed improvements are not due to random variation.

Author name	Parameter	Present study (WLHP-PE)	Published study
Usmani et al.[19]	Temperature reduction	8–10 °C	Temperature reduction of 6 °C using thermosyphon heat pipes
Arifin et al.[22]			> 10 °C using aluminium heat sinks
Yang et al.[15]	Efficiency improvement	10.2% → 11.4% (≈ 11.7%)	10–12% using pulsating heat pipes with PCM
Kianifard et al.[26]			Up to 15% with PV/T collector system
Arifin et al.[22]	Power output increase	122.13 W → 166.98 W (≈ 36.7%)	18.6% maxi power increase with aluminium heat sinks
Bizzy et al.[24]			120% increase in current output using perforated aluminium plate
Hudișteanu et al.[36]	Cooling mechanism	Wickless loop heat pipe (passive)	Pulsating heat pipe, PCM, aluminium heat sink

Table 9. A comparison between the current findings and previous published studies.

Data availability

The datasets generated during and/or analysed during the current study are available from the corresponding author on reasonable request.

Received: 27 March 2025; Accepted: 2 September 2025
Published online: 13 October 2025

References

1. Zaghloul, H., Emam, M., Abdelrahman, M. A. & Abd Rabbo, M. F. Optimization and parametric analysis of a multi-junction high-concentrator PV cell combined with a straight fins heat sink. *Energy. Conv. Manag.* **243**, 114382 (2021).
2. Dhairiyasamy, R. et al. Enhancing thermal efficiency in flat plate solar collectors through internal barrier optimization. *Therm. Sci. Eng. Prog.* **54**, 102856. https://doi.org/10.1016/j.tsep.2024.102856 (2024).
3. Pérez-Fargallo, A., Bienvenido-Huertas, D., Contreras-Espinoza, S. & Marín-Restrepo, L. Domestic hot water consumption prediction models suited for dwellings in central-southern parts of Chile. *J. Building Eng.* **49**, 104024 (2022).
4. Kapsalis, V., Kyriakopoulos, G., Zamparas, M. & Tolis, A. Investigation of the photon to charge conversion and its implication on photovoltaic cell efficient operation. *Energies* **14**(11), 3022 (2021).

5. Anand, A., Shukla, A., Panchal, H. & Sharma, A. Thermal regulation of photovoltaic system for enhanced power production: a review. *J. Energy Storage*. **35**, 102236 (2021).
6. Han, C. Simulation of series resistance increase through solder layer cracking in Si solar cells under thermal cycling. *Energies* **16**(6), 2524 (2023).
7. Mussard, M., Riise, H. N., Wiig, M. S., Rønneberg, S. & Foss, S. E. Influence of temperature coefficient and sensor choice on PV system performance. *IEEE J. Photovolt.* (2023).
8. Abdallah, R., Haddad, T., Zayed, M., Juaidi, A. & Salameh, T. An evaluation of the use of air cooling to enhance photovoltaic performance. *Therm. Sci. Eng. Progress*. **47**, 102341 (2024).
9. Wang, T., Zhao, J., Liu, W., Ma, L. & Liu, Z. Experimental investigation for the loop heat pipe with a bifacial flat evaporator. *Int. J. Therm. Sci.* **200**, 108989 (2024).
10. Zhang, Z. et al. Simulation of heat and mass transfer process in a flat-plate loop heat pipe and experimental comparison. *Appl. Therm. Eng.* **220**, 119705 (2023).
11. Waqas, A., Ji, J., Xu, L., Ali, M. & Alvi, J. Thermal and electrical management of photovoltaic panels using phase change materials–A review. *Renew. Sustain. Energy Rev.* **92**, 254–271 (2018).
12. Hooman, K., Huang, X. & Jiang, F. Solar-enhanced air-cooled heat exchangers for geothermal power plants. *Energies* **10**(10), 1676 (2017).
13. Qu, H., Gao, B., Kong, Q. & Xu, Z. Experimental study of the effect of ambient temperature on the output characteristics of PV-PCM systems. *J. Energy Storage*. **88**, 111535 (2024).
14. Murali, G. et al. Improved solar still productivity using PCM and nano-PCM composites integerated energy storage. *Sci. Rep.* **14**(1), 15609 (2024).
15. Yang, C. et al. Thermal evaluation of photovoltaic panels combined pulsating heat pipe with phase change materials: numerical study and experimental validation. *Energy Build.* **303**, 113806 (2024).
16. Elavarasan, R. M., Nadarajah, M., Pugazhendhi, R. & Gangatharan, S. An experimental investigation on coalescing the potentiality of PCM, fins and water to achieve sturdy cooling effect on PV panels. *Appl. Energy*. **356**, 122371 (2024).
17. El Kassar, R., Al Takash, A., Faraj, J., Khaled, M. & Ramadan, H. S. Phase change materials for enhanced photovoltaic panels performance: a comprehensive review and critical analysis. *Energy Built Environ.* (2024).
18. Chibani, A., Merouani, S., Laidoudi, H., Dehane, A. & Bougriou, C. Thermal management and electrical efficiency for concentrator photovoltaic systems using multiple phase change materials. *Appl. Therm. Eng.* **240**, 122207 (2024).
19. Usmani, M. K. & Deshmukh, S. P. Experimental study on performance improvement of photovoltaic panels using thermosyphon heat pipes. *Int. J. Energy Convers.* **11**(6) (2023).
20. Elsheniti, M. B., Hemedah, M. A., Sorour, M. M. & El-Maghlany, W. M. Novel enhanced conduction model for predicting performance of a PV panel cooled by PCM. *Energy. Conv. Manag.* **205**, 112456 (2020).
21. Qeays, I. A., Yahya, S. M., Asjad, M. & Khan, Z. A. Multi-performance optimization of nanofluid cooled hybrid photovoltaic thermal system using fuzzy integrated methodology. *J. Clean. Prod.* **256**, 120451 (2020).
22. Arifin, Z. et al. Numerical and experimental investigation of air cooling for photovoltaic panels using aluminum heat sinks. *Int. J. Photoenergy*. **2020**(1), 1574274 (2020).
23. Ma, T., Li, Z. & Zhao, J. Photovoltaic panel integrated with phase change materials (PV-PCM): technology overview and materials selection. *Renew. Sustain. Energy Rev.* **116**, 109406 (2019).
24. Bizzy, I. & Mustafrizal, L. PV panel cooler to enhance output performance using perforated aluminium plate. In *Journal of Physics: Conference Series*, Vol. 1198, No. 4, 042003 (IOP Publishing, 2019).
25. Yousefnejad, R., Atabaki, N. & Chiao, M. An algorithm for designing a cooling system for photovoltaic panels. *Sol. Energy*. **194**, 450–460 (2019).
26. Kianifard, S., Zamen, M. & Nejad, A. A. Modeling, designing and fabrication of a novel PV/T cooling system using half pipe. *J. Clean. Prod.* **253**, 119972 (2020).
27. Osma-Pinto, G. & Ordóñez-Plata, G. Dynamic thermal modelling for the prediction of the operating temperature of a PV panel with an integrated cooling system. *Renew. Energy*. **152**, 1041–1054 (2020).
28. Nazari, M. A., Ghasempour, R., Ahmadi, M. H., Heydarian, G. & Shafii, M. B. Experimental investigation of graphene oxide nanofluid on heat transfer enhancement of pulsating heat pipe. *Int. Commun. Heat Mass Transfer*. **91**, 90–94 (2018).
29. Nazari, M. A. et al. A review on pulsating heat pipes: from solar to cryogenic applications. *Appl. Energy*. **222**, 475–484 (2018).
30. Ahmadi, M. H. et al. Applicability of connectionist methods to predict thermal resistance of pulsating heat pipes with ethanol by using neural networks. *Int. J. Heat Mass Transf.* **126**, 1079–1086 (2018).
31. Song, Y. J. et al. Solar photo-voltaic and thermal (PVT) system facilitated with novel coaxial condensing heat pipe (CCHP): thermo hydrodynamic modelling and parametric optimization for overall operation performance. *Sol. Energy*. **264**, 112019 (2023).
32. Ahmad, T., Sobhan, S. & Nayan, M. F. Comparative analysis between single diode and double diode model of PV cell: concentrate different parameters effect on its efficiency. *J. Power Energy Eng.* **4**(3), 31–46 (2016).
33. Anderson, W. G., Dussinger, P. M., Sarraf, D. B. & Tamanna, S. Heat pipe cooling of concentrating photovoltaic cells. In *2008 33rd IEEE Photovoltaic Specialists Conference*, 1–6 (IEEE, 2008).
34. Senthil, R. et al. A holistic review on the integration of heat pipes in solar thermal and photovoltaic systems. *Sol. Energy*. **227**, 577–605 (2021).
35. Kagan J. Payback Period. Payback period: Definition, formula, and calculation. Investopedia. Retrieved September 2024, from https://www.investopedia.com/terms/p/paybackperiod.asp
36. Hudișteanu, S. V. et al. Enhancement of PV panel power production by passive cooling using heat sinks with perforated fins. *Appl. Sci.* **11**(23), 11323 (2021).

Author contributions

N.N, S.K.R Conceptualization, Methodology & Formal analysis, Writing – original draft, J.N, G.M, E.P.V, M.M Conceptualization, Methodology, Formal analysis, Writing – review & editing. P.S , Z.J, Methodology, G.M, Z.J Writing – review & editing.

Declarations

Competing interests

The authors declare no competing interests.

Additional information

Correspondence and requests for materials should be addressed to S.P.

Reprints and permissions information is available at www.nature.com/reprints.

Publisher's note Springer Nature remains neutral with regard to jurisdictional claims in published maps and institutional affiliations.

Open Access This article is licensed under a Creative Commons Attribution-NonCommercial-NoDerivatives 4.0 International License, which permits any non-commercial use, sharing, distribution and reproduction in any medium or format, as long as you give appropriate credit to the original author(s) and the source, provide a link to the Creative Commons licence, and indicate if you modified the licensed material. You do not have permission under this licence to share adapted material derived from this article or parts of it. The images or other third party material in this article are included in the article's Creative Commons licence, unless indicated otherwise in a credit line to the material. If material is not included in the article's Creative Commons licence and your intended use is not permitted by statutory regulation or exceeds the permitted use, you will need to obtain permission directly from the copyright holder. To view a copy of this licence, visit http://creativecommons.org/licenses/by-nc-nd/4.0/.

© The Author(s) 2025